Wang Yi (Orcid ID: 0000-0001-5633-3312)
Hendy Ingrid (Orcid ID: 0000-0001-8305-6752)
Thunell Robert (Orcid ID: 0000-0001-7052-1707)

Local and remote forcing of denitrification in the Northeast Pacific for the last 2000 years

Yi Wang[1], Ingrid L. Hendy[1], Robert Thunell[2]

[1]Department of Earth and Environmental Sciences, University of Michigan, Ann Arbor, MI, United States

[2]School of Earth, Ocean and Environment, University of South Carolina, Columbia, SC, United States

Corresponding author: Yi Wang (ellawang@umich.edu)

Key Points

- Wind-curl upwelling contributes to Southern California primary productivity, especially during weak coastal upwelling intervals.
- Intensified NPH leads to stronger denitrification through enhanced coastal upwelling and reduced rainfall.
- California receives relatively more tropical water during the Medieval Climate Anomaly, and more subarctic water during the Little Ice Age.

This is the author manuscript accepted for publication and has undergone full peer review but has not been through the copyediting, typesetting, pagination and proofreading process, which may lead to differences between this version and the Version of Record. Please cite this article as doi: 10.1029/2019PA003577

Abstract

Sedimentary $\delta^{15}N$ ($\delta^{15}N_{sed}$) has been widely applied as a proxy for water-column denitrification. When combined with additional productivity proxies, it provides insights into the driving forces behind long-term changes in water column oxygenation. High-resolution (~2 years) $\delta^{15}N_{sed}$ and productivity proxy records (total organic carbon [TOC], Si/Ti and Ca/Ti) from Santa Barbara Basin, California were generated from a well-dated Kasten core (SPR0901-03KC). These records reveal the relationship between Southern California upwelling and oxygenation over the past 2000 years.

Inconsistencies between Si/Ti (coastal upwelling proxy) and TOC (total export productivity proxy) suggest wind-curl upwelling influenced Southern California primary productivity, especially during intervals of weak coastal upwelling. Coherence between $\delta^{15}N_{sed}$, TOC, and drought indicators supports a local control of $\delta^{15}N_{sed}$ by atmospheric circulation, as persistent Northerly Winds associated with an intensified North Pacific High pressure cell lead to enhanced coastal upwelling. In the northeast Pacific, $\delta^{15}N_{sed}$ is used as a water mass tracer of denitrification signals transported north from the Eastern Tropical North Pacific (ETNP) via the California Undercurrent. A 1200-year $\delta^{15}N_{sed}$ record from the Pescadero slope, Gulf of California lies between denitrifying subsurface waters in the ETNP and Southern California. During the Medieval Climate Anomaly, coherence between Pescadero and SBB $\delta^{15}N_{sed}$ indicates connections between ETNP and Southern California on centennial time scales. Yet an out-of-phase relationship occurred when the Aleutian Low was anomalously strong during the Little Ice Age. We suggest intensified nutrient-rich subarctic water advection might have transported high-^{15}N nitrate into Southern California when the California Undercurrent and ETNP denitrification weakened.

1 Introduction

Highly active biogeochemical processes in oxygen minimum zones (OMZs) play a significant role in global nutrient cycling through their impact on nitrogen (N) cycles. In the three largest OMZs (eastern tropical North Pacific, eastern tropical South Pacific, and the Arabian Sea), water-column denitrification and anammox (anaerobic ammonium oxidation) observed at ~200-800 m (Brandes et al., 1998) account for almost a half of the total oceanic N loss (Ganeshram et al., 2002; Ganeshram et al., 1995). Thus, OMZs cast control on global nutrients through the fixed N inventory and ocean nutrient limitation, contributing to the regulation of CO_2 levels (Altabet, 2006b; Altabet and François, 1994; Deutsch et al., 2004; Ganeshram et al., 2002; Kienast et al., 2002). OMZs are anticipated to expand in a warming world due to reduced gas solubility and intensified stratification of the water column, yet the brevity of O_2 concentration observations in these OMZs (<50 years) makes separating long-term (multidecadal to centennial) natural oceanic variability from anthropogenic influences difficult.

OMZ intensity controls water-column denitrification, as nitrate becomes the favorable electron acceptor after dissolved O_2 is depleted in microbe-regulated organic carbon remineralization. $\delta^{15}N$ is widely accepted as a proxy for water-column denitrification (Altabet et al., 1995; Altabet et al., 1999a; Thunell et al., 2004). Preferential removal of ^{14}N by denitrification progressively enriches ^{15}N in the remaining subsurface nitrate pool, which is then advected throughout the ocean. When this $\delta^{15}N$-enriched nitrate is upwelled into the photic zone and incorporated in particulate organic carbon that is exported to the sea floor, the subsurface $\delta^{15}N$ signal is preserved in the sediments, leading to elevated sedimentary $\delta^{15}N$ (Altabet, 2006b; Altabet and François, 1994; Deutsch et al., 2004; Ganeshram et al., 2002; Kienast et al., 2002). When O_2 supplies are reduced (e.g. due to lower solubility in a warmer climate) and/or O_2 consumption increases (e.g. due to greater availability of organic carbon for remineralization), sedimentary $\delta^{15}N$ increases alongside intensified water-column denitrification. To use $\delta^{15}N$ as an indicator of O_2 concentration, complete nitrate

utilization in the photic zone must occur and $\delta^{15}N$ cannot be compromised during sedimentary diagenesis (Prokopenko et al., 2006; Thunell et al., 2004). Incomplete nitrate consumption in the photic zone, however, leaves a high $\delta^{15}N_{nitrate}$ signature due to preferential uptake of ^{14}N in photosynthesis, complicating sedimentary $\delta^{15}N$ interpretations (Altabet and François, 1994). The relative contribution of different N sources may also alter $\delta^{15}N$ of the fixed N pool and sedimentary $\delta^{15}N$ records (Fig. 2). Although oceanic N is usually sourced from N fixation ($\delta^{15}N$ = -2-0‰), atmospheric deposition ($\delta^{15}N \approx$ -2‰), and terrestrial input ($\delta^{15}N \approx$ 4‰) (Altabet, 2006b; Sigman et al., 2009a), increasing anthropogenic atmospheric deposition can decrease surface water $\delta^{15}N$ (Ren et al., 2017), and $\delta^{15}N$-depleted terrestrial inorganic carbon input can bias sedimentary $\delta^{15}N$ towards lower values (Kienast et al., 2005). Additionally, remotely advected water masses with different $\delta^{15}N$ signatures supply extra N to the photic zone in upwelling regions (e.g., Southern California margin; Liu and Kaplan (1989)), transmitting unique $\delta^{15}N$ signatures to sediments.

Previous studies have shown that >1‰ $\delta^{15}N$ shifts in the Arabian Sea and the east tropical north Pacific (ETNP) occurred between glacial and interglacial, as OMZs contracted during cool intervals and expanded as climate warmed (Altabet et al., 1995; Ganeshram et al., 1995; Pride et al., 1999). Although $\delta^{15}N$ is assumed to be relatively stable in the late Holocene (Altabet, 2006a), several millennial-scale $\delta^{15}N$ records have shown linkages between OMZ variability and the Intertropical Convergence Zone (ITCZ) migration (Agnihotri et al., 2008; Salvatteci et al., 2014). A more southerly ITCZ position associated with centennial/millennial-scale Northern Hemisphere (NH) cooling coincides with lower surface productivity and reduced denitrification off Peru (Agnihotri et al., 2008), supporting an oceanic OMZ response to climate forcing via large-scale atmospheric circulation.

A 2000-year high-resolution (~2 years) $\delta^{15}N_{sed}$ record from the well-dated Kasten core SPR0901-03KC (34°16.99’N, 120°2.408’W; 586 m depth) in the Santa Barbara

Basin (SBB), Southern California was generated to explore long-term natural variability of $\delta^{15}N$ in response to water-column oxygenation and/or N flux changes. Paired total organic carbon (TOC) and the scanning X-ray fluorescence (XRF) elemental analyses constrain the impacts of regional productivity and terrestrial N input on sedimentary $\delta^{15}N$. These records show coherence between $\delta^{15}N_{sed}$, export productivity, and local precipitation to reveal a local control of the Southern California denitrification. The SBB $\delta^{15}N_{sed}$ was also compared to the 1200-year $\delta^{15}N_{sed}$ record from the Pescadero slope, Gulf of California (Tems et al., 2016), and the Mt. Logan ice core record (Osterberg et al., 2014) to investigate the coherence of northeast Pacific $\delta^{15}N$ variability in response to larger-scale (regional or global) processes (e.g., tropical and extra-tropical forcing). We will demonstrate competing influences of high-$\delta^{15}N$ saline water from the ETNP OMZ and oxygenated fresh water from the subarctic ocean following multidecadal to centennial-scale climate change.

2 Background

The Santa Barbara Basin (SBB) is a semi-closed basin located on the Southern California margin. Sedimentation in SBB is associated with annual couplets formed by alternation of biogenic-rich (light laminae under the X-ray radiography) and siliciclastic-rich sediments (dark laminae under the X-ray radiography). The lithogenic component accounts for ~70-80% of SBB sediments (Thunell et al., 1995) and is delivered to the basin via rivers draining the Western Transverse Ranges (Hendy et al., 2015). Under California's Mediterranean climate, the North Pacific High (NPH) weakens and is displaced equatorward in winter, allowing a strengthened Aleutian Low (AL) to steer precipitation toward Southern California, driving increased river runoff and silicilastic sedimentation (Checkley and Barth, 2009; Warrick and Farnsworth, 2009a).

In spring and summer, the NPH strengthens and migrates poleward, resulting in strong east-west pressure gradients that drive northerly upwelling-favorable alongshore

winds, generating strong coastal upwelling (Checkley and Barth, 2009; Chelton, 1981). Nutrient-rich subsurface water upwells along the coast, producing spring-summer plankton blooms. In addition to coastal upwelling that is typically restricted within 5-30 km along the coast (Checkley and Barth, 2009), offshore upwelling (up to 200 km) also plays a role in generating the high productivity observed in SBB. In the Southern California Current System (CCS), negative wind-curl in the North Pacific subtropical gyre is balanced by the positive wind-stress curl near-shore (Checkley and Barth, 2009; Pickett, 2003; Rykaczewski and Checkley, 2008). Upwelling driven by the positive wind-curl usually has much lower velocities (0.1-0.2 m/d vs. 10-20 m/d for coastal upwelling) (Pickett, 2003). However, the volume transport of wind-curl upwelling is significant due to greater areal extent (Chelton et al., 2007; Jacox et al., 2014; Münchow, 2000). Together, coastal upwelling and wind-curl upwelling in SBB result in the annual formation of biogenic-rich sediment layers during times of NPH dominance. Finally, low O_2 bottom water (<20 µmol/kg) preserves varves formed by the seasonal shift between biogenic and silicilastic sedimentation (Hendy et al., 2015; Schimmelmann et al., 1992; Schimmelmann et al., 1990), while high sedimentation rates (~1 mm/y) minimize sedimentary diagenesis, such that SBB sediments retain the original subsurface $\delta^{15}N$ signal (Prokopenko et al., 2006).

SBB waters are affected by the equatorward California Current (CC) and poleward California Undercurrent (CUC) (Fig. 1). As a part of the North Pacific Gyre, the CC originates in the bifurcation of the North Pacific Current (NPC) (Checkley and Barth, 2009). Occupying the upper 500 m and strongest at the surface, the CC transports cold, fresh, and oxygenated water from the subpolar region (Checkley and Barth, 2009; Hickey, 1978). CC strength is connected to large-scale gyral circulation and atmospheric forcing (strength of the Trade Winds/Westerlies). When the NPC is stable, CC transport is generally anti-correlated with Alaska Current strength (Rykaczewski and Checkley, 2008). However, when the NPC intensifies, both CC and Alaska Current transport

increase, while when the NPC weakens, transport decreases (Cummins and Freeland, 2007). Most observed low-frequency CC variability is associated with NPC transport changes (Cummins and Freeland, 2007). Satellite altimetry reveals in-phase NPC strength and Ekman pumping variations in the subpolar and subtropical gyres (Cummins and Freeland, 2007), further linking CCS strength to gyral circulation behavior. Finally, where the NPC bifurcates on the North America margin affects SBB water properties, as a poleward displacement leads to transport of fresher, nutrient-rich water from the subpolar gyre into the CCS (Freeland and Cummins, 2005; Sydeman et al., 2011).

CUC is a subsurface poleward flow with a core depth of ~200-300 m occupying the nearshore region (within 25-40 km off the shelf break), which advects warm, salty, and low-oxygen water from the ETNP up the coast of North America (Hickey, 1978). Nutrient-rich CUC waters are upwelled to the surface along the coast, supporting biological productivity in the southern CCS (Hickey, 1978; McClatchie et al., 2016). Bi-annual CUC intensification is observed in June and December (Chelton, 1984; Lynn and Simpson, 1987) and was linked to local processes (upwelling-enhanced subsurface flow in spring-summer and the strong Southern California Eddies in winter) (Connolly et al., 2014; Hickey, 1978). Recent studies, however, indicate that coastal-trapped Kelvin waves control CUC intensity, which propagate a sea level signal from the equator, providing a further connection between the southern CCS and the Tropics (Gómez-Valdivia et al., 2015; Gómez-Valdivia et al., 2017).

3 Methods

Core SPR0901-03KC was scanned using an ITRAX X-ray fluorescence (XRF) core scanner (Cox Analytical Instruments) at the Large Lakes Observatory, University of Minnesota, Duluth. The scanner was equipped with a Cr X-ray tube and was operated at 200-µm resolution with an 8-second scan time at 30 kV and 15 mA. The output data are recorded as counts per 8 seconds and are semi-quantitative (Croudace et al., 2006; Hendy

et al., 2015). A split of SPR0901-03KC was sampled continuously at 2-mm interval (~2 years per sample). Individual samples were freeze-dried and ground to produce bulk samples for $\delta^{15}N$ and TOC measurements. Bulk sedimentary $\delta^{15}N$ was measured on a Euro Elemental Analyzer interfaced to a GV Isoprime continuous flow isotope-ratio mass spectrometer (IRMS) at University of South Carolina on unacidified samples. $\delta^{15}N$ is defined as $[(^{15}N/^{14}N_{sample})/(^{15}N/^{14}N_{standard})-1]\times1000$ with the standard of atmospheric N_2. The reference standards used for data normalization were N-1 ($\delta^{15}N$ = 0.4‰), N-2 ($\delta^{15}N$ = 20.41‰), N-3 ($\delta^{15}N$ = 4.7‰), and USGS-40 ($\delta^{15}N$ = -4.52‰). For TOC measurements, ~250 mg aliquots were acidified to remove carbonate with 10 mL 5% HCl on a 50 °C hotplate for three times. Acidified samples were oven-dried at 65 °C for at least 48 hrs and then ground for TOC measurements. Eight to 12 mg of acidified samples were loaded into tin capsules and measured on a Costech ECS 4010 Elemental Analyzer at University of Michigan. Acetanilide (C = 71.09 wt. %) and atropine (C = 70.56 wt.%) were used as standards, and the standard deviation of repeated measurements was within 2%. Flood and turbidite layers were removed from the geochemical time series as they do not reflect background marine sedimentation and siliciclastic sediment input causes significant dilution (Hendy et al., 2013).

The age model of SPR0901-03KC was constructed by correlation with nearby cores. Forty nine mixed planktonic foraminifera accelerator mass spectrometry (AMS) ^{14}C dates (Du et al., 2018; Hendy et al., 2013) from SPR0901-06KC (34°16.914’ N, 120°02.419’ W, 591 m water depth) were mapped on the master core SPR0901-03KC using sediment fabric characteristics. Varve counted dates of marker layers (e.g., gray layers at 1861-62 CE and 1761 CE, the *Macoma* layer at 1841 CE, and a turbidite layer at 1811 CE) were used instead of ^{14}C to constrain the past 300 years (Hendy et al., 2015; Schimmelmann et al., 1992). Instantaneous packets of sediments produced by floods and turbidites were removed from the core depths. An age-depth model for 03KC scanning XRF records was then generated using Bacon 2.2 (Blaauw and Christen, 2011; Du et al.,

2018), where ^{14}C ages were converted to calendar ages using the Marine13 calibration curves (Reimer et al., 2013) with variable reservoir ages from Hendy et al. (2013). This age model was then applied to the suite of SBB cores using 31 tie points including known turbidites, flood layers, and 12 visually distinct additional marker horizons determined by distinguishable core fabric differences (e.g., varve color and thicknesses).

Geochemical data were interpolated to obtain evenly spaced time series (sampling resolution of 2.28 years after interpolation) prior to statistical analyses. Cross-wavelet analysis was used to calculate squared wavelet coherence and phase differences on a time-frequency plane to reveal regional coherence between individual time series (Grinsted et al., 2004; Torrence and Compo, 1997) . All wavelet coherence is calculated using the analytical Morlet wavelet (central frequency $\omega_0 = 6$) in MATLAB.

4 Results

Bulk sedimentary $\delta^{15}N$ in the core SPR0901-03KC varies between 6.78‰ and 8.33‰ with a mean value of 7.74‰ (Fig. 3b). There is no long-term trend through the record; however, several low- $\delta^{15}N_{sed}$ intervals occur, including ~1000-1100 CE during the Medieval Climate Anomaly (MCA) and 1460-1750 CE during the Little Ice Age (LIA). $\delta^{15}N$ values decline from ~1800 to the core top (~1900 CE).

Bulk TOC concentrations are low at the base of the core (from 170 BCE to 0) with a minimum value of 2.63 wt.% (Fig. 3c), and generally increase toward the core top, varying between 4.89 wt.% and 3.77 wt.% (excluding instantaneous depositional events). TOC concentrations are not statistically significant different between cooler (e.g., Dark Age Cold Period at 400-765 CE (Helama et al., 2017) and LIA) and warmer climate intervals (e.g., MCA), yet they have a statistically significant correlation with $\delta^{15}N$ ($r = 0.0760$, $p<0.05$). Despite overall coherence, the positive correlation disappears between 950-1550 CE and after 1800s. The elemental, isotopic, and organic geochemical composition of organic carbon in SBB indicates marine sources with significant

contributions from terrestrial organic carbon, notably in flood sediments (Sarno et al., 2019). Background SBB sediment $\delta^{13}C$ values of -21.75‰ support a marine source, as terrestrial contributions (primarily from the Santa Clara River (Warrick and Farnsworth, 2009b) are characterized by bedload sediment $\delta^{13}C$ values of -28.15‰ (Meyers, 1997; Sarno et al., 2019).

The first principal component (PC1) of the scanning XRF elements in SPR0901-02KC has been used as a proxy for lithogenic sediment delivery to SBB by river runoff, with higher PC1 corresponding to wetter intervals (Fig. 3a) (Heusser et al., 2015). PC1 is anti-correlated with TOC ($r = -0.4004$, $p < 0.0001$), and has a statistically significant negative correlation with $\delta^{15}N_{sed}$ ($r = -0.1617$, $p < 0.001$). Stronger coherence between PC1 and $\delta^{15}N_{sed}$ is observed during wetter intervals (50-100 CE, 950-1130 CE, 1530-1700 CE), whereas the correlation is lost during drier periods (770-1000 CE). This negative correlation also disappears after ~1800 as $\delta^{15}N_{sed}$ decreases monotonically (Fig. 3a and b).

Scanning XRF elemental records of Ca/Ti and Si/Ti are used here as proxies for inorganic carbon (Hendy et al., 2015) and biogenic silica (Brown et al., 2007), respectively. Ca/Ti varies on a decadal to centennial time scale but no longer-term trend is observed. Several low biogenic silica periods are observed in the Si/Ti record, including 450-890, 1000-1100, 1150-1260, 1310-~1370, and 1520-1650 CE (Fig. 4e). These intervals correspond to intervals of low upwelling silicoflagellate (*Distephanus speculum*) and diatom (*Rhizosolenia spp*.) abundance (Barron et al. (2015), Fig. 4d). A significant positive correlation is found between Ca/Ti and TOC ($r = 0.3532$, $p < 0.001$). High Si/Ti (high biogenic silica) generally coincides with increased TOC (e.g., ~1100-1170 CE and ~870-1000 CE, Fig. 4). Yet a weak anti-correlation is observed between TOC and Si/Ti ($r = -0.0941$, $p < 0.05$), notably between 570-970, 1000-1100, 1150-1270, and 1320-1370 CE.

5 Discussions

5.1 Export productivity proxies and upwelling

In Southern California, upwelling (coastal and wind-curl) brings subsurface high-nutrient denitrified waters to the euphotic zone to support export productivity. Water-column denitrification (increasing $\delta^{15}N$) is subsequently intensified by increased export productivity when organic carbon remineralization uses nitrate as the electron acceptor in low-O_2 waters. Export productivity and upwelling variability thus need to be reconstructed using biogenic sediments (e.g., TOC, biogenic carbonate and silica) to understand local water-column denitrification.

TOC is commonly employed as a proxy for carbon export from the upper ocean. An overall increase of TOC (~1 wt. %) occurs over the last two millennia, indicating a general increase in export productivity, with significant variability on centennial timescales (Fig. 3c). However, the bulk sediment TOC concentration could subject to sedimentary diagenesis, causing the record to deviate from carbon export. In high-sedimentation rate settings (>0.03 cm/y, Canfield (1994)), OC could continue to decompose downcore via anaerobic pathways in reducing porewaters, leading to lower sedimentary TOC (Canfield et al., 1993). Additionally, higher TOC values (enhanced OC preservation) could occur beneath instantaneous depositional events (e.g., flood and turbidite layers) that reduce O_2 penetration and aerobic OC degradation (i.e., the 'coffin-lid' effect, Schimmelmann (2011)).

To exclude the fore-mentioned complexities, an independent export productivity indicator is needed to account for likely diagenetic processes affecting TOC records. Inorganic carbon determined by scanning XRF Ca/Ti is a productivity proxy representing biogenic carbonate production (primarily foraminifera and coccolithophores, Fig. 4c). In SBB, well-preserved inorganic carbon is unaffected by sedimentary anaerobic OC degradation and/or enhanced OC preservation, and thus provides an independent measure of export productivity that can be compared to TOC. Ca/Ti and TOC are generally

coherent on decadal to centennial timescales. This statistically significant correlation ($r = 0.3532$, $p < 0.01$) suggests TOC preservation below instantaneous deposition events was not enhanced, nor were there significant changes in TOC anaerobic decomposition downcore. Thus, sedimentary TOC is likely primarily recording export productivity in SBB.

Additionally, biogenic silica (largely produced by diatoms and silicoflagellates) is another major contributor to export productivity, especially during coastal upwelling events. Scanning XRF Si/Ti is used here as a proxy for biogenic silica, with the expectation that higher Si/Ti corresponds to enhanced export productivity. Coherent TOC and Si/Ti maxima are observed (e.g., 1130 and 1300 CE), yet negative correlations between Si/Ti and TOC are shown during intervals of low Si/Ti, during which TOC remains relatively stable (Fig. 4b and e). Anti-correlations between TOC and biogenic silica have also been recorded in the Gulf of California, where biogenic silica is the primary biogenic sediment component (Pichevin et al., 2012; Thunell, 1998b). Previous studies have related this inverse relationship to either Fe limitation (Firme et al., 2003) and/or enhanced silica preservation during strong coastal upwelling events due to silica supersaturation in porewaters (Pichevin et al., 2012). However, SBB sediments are dominated by lithogenic input (50-80%), with much lower biogenic silica contributions (~15%-20% in SBB vs. up to ~75% during upwelling in the Guaymas Basin, Gulf of California) (Thunell, 1998a; Thunell, 1998b). Thus, SBB porewaters are always undersaturated for silica, as indicated by the absence of weakly silicified species (Barron et al., 2015; Reimers et al., 1990). Iron limitation due to upwelled Fe-depleted waters and/or low riverine input usually occurs along narrow shelf areas (e.g., the northern and central California coast) (Bruland et al., 2001; Firme et al., 2003). However, relatively high dissolved Fe (dFe) concentrations (>1 nM) have been observed at the surface in SBB with increasing dFe in depth (up to ~30 nM at 560 m), arguing against reduced organic carbon production because of Fe limitation (John et al., 2012; King and Barbeau,

2011). Therefore, the lack of TOC and biogenic silica correspondence in SBB requires another explanation.

In the Gulf of California, negative correlations between biogenic silica and TOC usually happen during intervals associated with strong coastal upwelling (Pichevin et al., 2012) In SBB, however, negative relationships are more prominent during weak biogenic silica production intervals indicated by the low abundance of coastal upwelling diatom (*Rhizosolenia* spp.) and silicoflagellate species (*Distephanus speculum*) (Fig. 4d) (Barron et al., 2015). Despite undersaturated porewaters leading to biogenic silica dissolution, Si/Ti shows consistent variability with independently measured upwelling diatoms and silicoflagellates. Sedimentary Si/Ti increases when *Rhizosolenia* spp. and *Distephanus speculum* become abundant at 1110-1160, 1270-1310, and 1370-1490 CE, supporting the interpretation of intensified coastal upwelling (Fig. 4d) (Barron et al., 2015). Low Si/Ti is coincident with a scarcity of these upwelling species during 570-870, 1000-1100, 1155-1265, and 1310-1370 CE, suggesting weakened coastal upwelling. Si/Ti thus appears to be an indicator of coastal upwelling but not necessarily export productivity, and can be decoupled from TOC when coastal upwelling is weak.

Nevertheless, anti-correlations between Si/Ti and TOC contradicts sediment trap studies in SBB, where export particulate organic carbon (POC) is positively correlated with opal fluxes on an annual basis (Thunell et al., 2007). This may relate to the limitation of the short duration sediment trap study. Weak coastal upwelling in the paleoproductivity record is sustained on decadal to centennial timescales, such that this observed low-frequency variability might be associated with processes that have not yet been observed in the annual trap data.

When biogenic silica indicates weak coastal upwelling, Ca/Ti and TOC support normal to increased productivity (e.g., 1000-1100 and 1310-1370 CE, Fig. 4b, c, and e), indicating that nutrients are being supplied by processes other than coastal upwelling. Discrepancies between high foraminifera production and biogenic silica were also

observed in the northern CCS during the Last Glacial Maximum, and were attributed to increased wind-curl upwelling (Ortiz et al., 1997). Coastal upwelling is usually associated with high nutrient delivery due to high vertical velocity and a shoaling of the nearshore nutricline (Rykaczewski and Checkley, 2008; Taylor et al., 2015a), producing diatom blooms (high Si/Ti) and physically larger plankton. In the southern CCS, modeled total upwelling transport (including both coastal and wind-curl upwelling), however, is not significantly correlated with the coastal upwelling index calculated from atmospheric sea level pressure (Bakun, 1973). Rather, the nearshore high primary productivity band contains both coastal (<50 km) and wind-curl upwelling nutrient contributions (50-200 km) (Jacox et al., 2014).

The contribution of wind-curl upwelling is difficult to reconstruct, as the bloom-forming taxa associated with strong coastal upwelling events (e.g., upwelling diatoms that favor high nutrient environments) can overprint physically smaller planktonic taxa that dominate offshore and more oligotrophic environments associated with slow and broad wind-curl upwelling (Ortiz et al., 1995). Yet, the importance of wind-curl upwelling on southern CCS planktic biomass is widely reported. Wind-stress modeling shows strong wind-curl upwelling transport adjacent to coastal promontories (e.g., Point Conception) (Pickett, 2003) – a prediction corroborated by wind stress and upwelling rate observations (Enriquez and Friehe, 1995). The biological significance of wind-curl upwelling has been observed in seasonal offshore (100 km) zooplankton abundances (Chelton et al., 1982). Chlorophyll *a* concentrations (proxy for primary productivity) are significantly correlated with the wind-curl upwelling but not the coastal upwelling rate, and corroborate the active role of curl-driven upwelling in Southern California primary productivity (Rykaczewski and Checkley, 2008). Wind-curl upwelling could thus be an important driver of export productivity in SBB over the last 2000 years, such that intervals of weaker coastal upwelling (low Si/Ti) may have been offset by greater wind

curl upwelling to maintain stable/high export productivity (TOC and inorganic carbon) (Fig. 4).

5.2 Santa Barbara Basin $\delta^{15}N$ history over the past 2000 years

Use of $\delta^{15}N_{sed}$ as a proxy for water column denitrification requires both complete nitrate utilization and the absence of sedimentary diagenesis. Diagenetic isotopic alteration of $\delta^{15}N$ should be negligible in SBB as high sedimentation rates and low-oxygen bottom waters only allow a small fraction of aerobic OC decomposition before burial (Altabet et al., 1999b; Prokopenko et al., 2006). A minimal (<0.5‰) offset between the sediment trap $\delta^{15}N$ time series and down-core $\delta^{15}N_{sed}$ records supports this premise (Davis et al., 2019). Preservation of the original $\delta^{15}N$ of sinking OC thus allows water-column denitrification reconstructions from the $\delta^{15}N_{sed}$ record in SBB. Resolution of our record (~2 years), however, is insufficient to resolve O_2 entrainment/solubility shifts induced by seasonal wind-driven mixing/upwelling oscillations. Our $\delta^{15}N_{sed}$ record, therefore, can only reveal water-column $\delta^{15}N$ variability averaged over decadal or longer timescales.

Despite an ~1 wt.% increase of TOC over the last 2000 years (Fig. 3c), relatively invariant $\delta^{15}N_{sed}$ values (varying within ~1‰) indicate a general stability of water-column oxygenation and/or $\delta^{15}N$ input from different N sources. Exceptions to this stability occurred, however. Sustained low $\delta^{15}N_{sed}$ values during ~1100-1300, 1460-1750 CE, and after 1800s (>1‰ decline), suggesting the presence of more oxygenated waters or increasing $\delta^{15}N$-depleted N inputs (Fig. 3b). The post-1800s decreasing $\delta^{15}N_{sed}$ trend has also been observed in the Santa Monica Basin and in the ETNP, where it has been associated with decreasing trade wind strength, reduced equatorial upwelling, and ETNP OMZ contraction (Davis et al., 2019; Deutsch et al., 2014). The stability of the $\delta^{15}N_{sed}$ record suggests that denitrification appears insensitive to SST change during the warm (MCA) and cold periods (Dark Age Cold Period (DACP) or LIA) in the late Holocene (Fig. 3; PAGES 2k Consortium (2013)). This may be related to limited Northern

Hemisphere mean SST variability (typically < 1 °C for LIA, Moberg et al. (2005)), resulting in a gas solubility change (~ 5 μmol/kg given 1 °C SST change at 16 °C) that was insufficient to impact O_2 concentrations and thus denitrification.

Low $\delta^{15}N_{sed}$ intervals (~1100-1300 CE, 1460-1750 CE) are usually coincident with high values of the first principle component of the scanning XRF elements (PC1; Fig. 3, r = -0.1617, p < 0.001), which have been associated with greater Southern California rainfall (Hendy et al., 2015; Heusser et al., 2015). This anti-correlation may be related to changes in N source between wet and dry climates as enhanced clay-bound N delivery adds $\delta^{15}N$-depleted ammonium (~2-4‰; Schubert and Calvert (2001); Sigman et al. (2009b)) that may substitute for K^+ in illite clay structures (Kienast et al., 2005; Müller, 1977; Schubert and Calvert, 2001). Yet the TOC-TN plot (Fig. 5) shows a negative intercept, indicating that the contribution from terrestrial clay-bound N is negligible.

More likely, the relationship between rainfall (PC1) and $\delta^{15}N_{sed}$ is indirect via the North Pacific High (NPH), and related to export productivity. The positive correlation between bulk sedimentary TOC (export productivity proxy) and $\delta^{15}N_{sed}$ (r = 0.0760, p<0.05) indicates a general productivity control on water-column denitrification, with enhanced OC export increasing O_2 demand and thus denitrification. The negative correlation between TOC and PC1 (r = -0.4004, p<0.001) further suggests an inverse relationship between export productivity and local precipitation that is controlled by the NPH. A stronger and/or more persistent NPH enhances alongshore northerly winds, which induce stronger coastal upwelling and the upward advection of $\delta^{15}N$-rich subsurface waters to support higher export productivity (higher TOC, Fig. 3). Simultaneously, this persistent high-pressure over western North America reduces rainfall in Southern California and lowers PC1, leading to a negative correlation between PC1 and TOC (Hendy et al., 2015; Heusser et al., 2015). Despite the overall local productivity control on $\delta^{15}N_{sed}$ via the NPH, TOC, $\delta^{15}N_{sed}$ and PC1 still show

discrepancies (notably in 750-1250 and 1700-1900 CE), indicating that remote processes/teleconnections must have also played a role.

5.3 Teleconnections to tropical and high-latitude forcing

Inconsistencies between $\delta^{15}N_{sed}$ and local NPH control on export productivity (TOC) and precipitation (PC1) require an alternative explanation involving remotely advected $\delta^{15}N$ signals via ocean currents. Currents transport nitrate with unique $\delta^{15}N$ signatures from remote water sources. The nitrate is subsequently incorporated into sinking particulate N and preserved in sediments (Fig. 2), and thus $\delta^{15}N_{sed}$ can be used as a water mass tracer to track N contribution changes from different sources. In Southern California, water mass properties are primarily controlled by two competing water mass influences: high-$\delta^{15}N$, warm, saline (spicy) waters from the East Tropical North Pacific (ETNP) OMZ transported by the California Undercurrent (CUC), as well as nutrient-rich, cold, and fresh subarctic waters advected by the California Current (CC) (Kienast et al., 2002; Liu and Kaplan, 1989) (Fig. 2). To investigate impacts of remote water mass advection, the Mt. Logan in Yukon Territory (a high-latitude site) and the Pescadero Slope in the Gulf of California (a tropical site) are used as potential regions communicating with the Southern California OMZ (Fig. 1). The 1200-year $\delta^{15}N_{sed}$ record from the Pescadero Slope serves as an end member for ETNP $\delta^{15}N$-rich spicy water, as the site is located at the northern edge of the ETNP OMZ and records water-column denitrification in the ETNP (Tems et al., 2016). The competing subpolar end member is represented by the 1200-year North Pacific Index (NPI) reconstruction from the Mt. Logan ice core (Osterberg et al., 2014). Sodium ion concentrations in the Mt. Logan ice core are interpreted as an indicator of the North Pacific sea level pressure and winter Aleutian Low (AL) intensity (Osterberg et al., 2014). Thus, we use the ice core record to link the atmospheric forcing (AL intensity) with the oceanic responses (Ekman pumping and North Pacific Current variability) (Ishi and Hanawa, 2005) that result in subarctic

water transport into the CCS. Here the focus is on decadal to centennial timescales, as the data resolution (~2-3 years for $\delta^{15}N$) is insufficient to resolve interannual variability.

5.3.1 Equatorial water influences and atmospheric forcing

Spicy and high-$\delta^{15}N$ waters from ETNP could be advected to Southern California via CUC to elevate $\delta^{15}N_{sed}$ in SBB. A positive correlation between $\delta^{15}N$ from a SBB box core (SPR0901-04BC, 34º 16.895' N, 120º 02.489' W, 588 m water depth) and measured salinity at the core of CUC (σ_θ = 26.4-26.5, Gay and Chereskin (2009)) from the CalCOFI station 81.8 46.9 (center of SBB, 34°16´29.64"N, 120°1´30"W) during the last 50 years supports this assertion (Fig. 6).

Water-column denitrification ($\delta^{15}N$) in ETNP has been associated with tropical climate through Trade Wind strength (Deutsch et al., 2014). Weak easterly Trade Winds reduce upwelling and lower export productivity, leading to ETNP OMZ contraction that subsequently reduces $\delta^{15}N$. The strength of Trade Winds is related to ITCZ migration in response to inter-hemispheric temperature differences. A southward shift of the ITCZ with extratropical cooling in the Northern Hemisphere (NH) relative to the Southern Hemisphere (SH) is usually accompanied by intensified northeast Trades in the NH and weakened southeast Trades in the SH (Broccoli et al., 2006; Chiang and Bitz, 2005; Haug et al., 2001; Jacobel et al., 2016; McGee et al., 2018; Meehl et al., 2008; Schneider et al., 2014). Because the ITCZ primarily resides in the NH (Philander et al., 1996; Xie, 1994), a southward ITCZ shift weakens the easterly Trades at the equator, deepening the thermocline and reducing upwelling in the Eastern Equatorial Pacific (Costa et al., 2017; Koutavas and Lynch-Stieglitz, 2004).

The linkage between ITCZ migration and ETNP $\delta^{15}N$ is further demonstrated by the relationship between Pescadero Slope $\delta^{15}N_{sed}$ values and a $\delta^{18}O$ speleothem record (YOK-I) from Belize that is sited on the northern edge of the ITCZ (Kennett et al., 2012). From 1850 to 2004, YOK-I $\delta^{18}O$ values significantly correlate with Pescadero $\delta^{15}N$

values (Fig. 7, $r = -0.5494$, $p < 0.001$). The observed southward displacement of ITCZ since ~1850 (Hwang et al., 2013; Ridley et al., 2015; Rotstayn and Lohmann, 2002) could have slackened east Trades and weakened upwelling at the equator, reducing export productivity and decreasing Pescadero $\delta^{15}N_{sed}$ (a record that represents ETNP $\delta^{15}N$). Cross-wavelet coherence between the two records further indicates significant anti-phase coherence on decadal (~1100-1300 CE) to centennial timescales (Fig. 8e), supporting a persistent linkage between ETNP $\delta^{15}N$ and the ITCZ over the past 1200 years (Fig. 8).

The SBB and Pescadero $\delta^{15}N_{sed}$ records are usually in-phase on decadal to centennial timescales during the MCA (e.g., 980-1120 CE, Fig. 8b and c). Thus the ITCZ position increased Southern California (SBB) $\delta^{15}N$ through the advection of denitrified ETNP waters in the region via the CUC during the warm Northern Hemisphere climate interval. However, this relationship collapses between ~1320-1450 and 1670-1880 CE (Fig. 8). The anti-phase correlation in 1320-1450 CE could be attributed to ^{14}C dating uncertainties producing a 20-30 year offset between the two records. Yet the out-of-phase pattern during 1670-1840 CE (1720-1840 CE in particular) cannot be explained by age model offsets given its duration of centuries. Coincident with NH cooling during the Maunder (1645-1715 CE) and Dalton (1790-1820 CE) solar minimum, the 1670-1840 CE interval stands out as a period of equatorward ITCZ migration (YOK-I $\delta^{18}O$; Kennett et al. (2012)) where the weakened ETNP OMZ resulted in low Pescadero $\delta^{15}N_{sed}$ values (Tems et al., 2016) (Fig. 8c and d), while SBB $\delta^{15}N_{sed}$ values increased (Fig. 8b). As Pescadero $\delta^{15}N_{sed}$ values are always higher than those in SBB, this out-of-phase pattern reduces the $\delta^{15}N$ difference between the two sites. One explanation could be enhanced poleward transport of ETNP waters to Southern California. However, an equatorward ITCZ displacement would have led to similar equatorward migration of the NPH and AL (Christoforou and Hameed, 1997; Lechleitner et al., 2017), suppressing coastal upwelling in Southern California while enhancing upwelling in the Gulf of California (Barron and

Bukry, 2007; Pérez-Cruz, 2017). Reduced the sea surface height at the southern boundary of CCS would decrease poleward CUC flow, producing a $\delta^{15}N$ result opposite to the one observed (Connolly et al., 2014; Taylor et al., 2015b). Another possibility is that during this interval of weak Southern California (SBB) and ETNP (Pescadero Slope) water mass communication, subarctic water influences became more prominent to produce the discrepancy between 1670 and 1840 CE.

5.3.2 Subarctic water transport and atmospheric forcing

Nutrient-rich subarctic water transported via CC is associated with the latitudinal position and intensity of the North Pacific Current (NPC) (Cummins and Freeland, 2007; Di Lorenzo et al., 2008; Freeland and Cummins, 2005; Sydeman et al., 2011). The CC intensifies following increased NPC transport (Cummins and Freeland, 2007; Douglass et al., 2006). Serving as the boundary between the Gulf of Alaska and northeast Pacific subtropical gyre, the strength of NPC is closely linked with in-phase variations of Ekman pumping in both gyres, and directly responds to atmospheric forcing (Cummins and Freeland, 2007). This co-variability of subpolar and subtropical gyres is similar to the North Pacific Gyre Oscillation (NPGO) proposed by Di Lorenzo et al. (2008), which has been used to explain nutrient variability in CCS. As no NPGO reconstruction is available for the last two millennia, the Mt. Logan ice core North Pacific Index (NPI) reconstruction is used instead as an indicator of winter AL intensity and thus is associated with Ekman pumping in the Gulf of Alaska (GoA) (Osterberg et al., 2014).

When the connection between Southern California (SBB) and ETNP (Pescadero Slope) was weak between 1670-1840 CE, an intensified winter AL suggested by the ice core record (Fig. 8a) (Osterberg et al., 2014) could have resulted in anomalous cyclonic wind stress curl and stronger Ekman upwelling in GoA. Stronger wind stress curl would in turn lead to intensified southward transport of subarctic water into the NPC and subsequently the CCS (Freeland, 2003; Murphree et al., 2003). A similar anomalous

southward intrusion of subarctic waters to CCS was observed in the 2002 summer, when the subarctic anomaly extended more than 1500 km along the US west coast, to at least 33°N (Bograd and Lynn, 2003; Huyer, 2003; Strub and James, 2003). Due to incomplete nitrate utilization in the subarctic ocean, nitrate $\delta^{15}N$ in the GoA photic zone is also elevated (up to 11‰ at the surface, Casciotti et al. (2002)). Increasing advection of nutrient-rich and high $\delta^{15}N$ subarctic water would then serve as another source of high-$\delta^{15}N$ nitrate for surface SBB waters. The observed correspondence between intensified AL and increased SBB $\delta^{15}N_{sed}$ thus indicates a stronger connection with the subarctic waters when the tropical influences weakened during the Little Ice Age (1670-1840 CE, Fig. 8).

5. Conclusions

Marine dissolved oxygen concentrations play an important role in biogeochemical cycles and can be impacted by climate changes. The high-resolution 2000-year sedimentary $\delta^{15}N$ ($\delta^{15}N_{sed}$) record from Santa Barbara Basin (SBB) reveals natural variability of Southern California water column oxygenation and highlights competition between tropical and subarctic water masses as surface ocean currents respond to climate forcing. Proxies for siliceous plankton bloom events (diatom and silicoflagellate populations, and scanning XRF Si/Ti) and export productivity (TOC) suggests that coastal upwelling and export productivity are not always in phase. This incoherence indicates a potential role for wind-curl upwelling in driving SBB primary productivity, especially during intervals of weak coastal upwelling. The correspondence of $\delta^{15}N_{sed}$ to export productivity (TOC) and local precipitation (PC1) indicates that an intensified and/or persistent North Pacific High (NPH) pressure cell was associated with enhanced export productivity during drought intervals.

Comparison with the Pescadero slope $\delta^{15}N_{sed}$ record in the Gulf of California (Tems et al., 2016) supports subsurface tropical water influences on the surface waters of

the Southern California Bight. The Pescadero $\delta^{15}N_{sed}$ record suggests that Eastern Tropical North Pacific (ETNP) denitrification was associated with Intertropical Convergence Zone migration on multidecadal to centennial timescales and supports the stronger tropical water transport into Southern California during the Medieval Climate Anomaly. An out-of-phase relationship between the Pescadero and SBB $\delta^{15}N_{sed}$ records during the Little Ice Age (1670-1840 CE) occurred during an interval of anomalous intensified Aleutian Low activity (Osterberg et al., 2014). During this interval we suggest that an intensified North Pacific Current advected more subarctic water into the California Current System. Enhanced advection of nutrient-rich subarctic waters might have introduced high-$\delta^{15}N$ nitrate to SBB, resulting in elevated SBB $\delta^{15}N_{sed}$ values while $\delta^{15}N_{sed}$ decreased at the Pescadero site.

The observed natural variability of water-column denitrification is associated with both local (export productivity shifts controlled by NPH) and remote water mass influences related to large-scale atmospheric forcing, and thus addresses regional teleconnections within the California Current System. A warming climate might lead to a strong, MCA-like connection between the Southern California margin and ETNP, with weaker influences from subpolar regions. Such natural oscillations would continue to be embedded in future climate change with anthropogenic forcing, which will further complicate predictions of future ocean deoxygenation.

Acknowledgments

This work is supported by the National Science Foundation under grant number OCE-1304327 awarded to I.H.; Y.W. acknowledges support from the Rackham Graduate School of the University of Michigan and the Scott Turner Award. We thank Eric Tappa, Alexander Postmaa, and Madeline Parks for lab assistance. $\delta^{15}N$ and total organic carbon data are included in the Supporting Information.

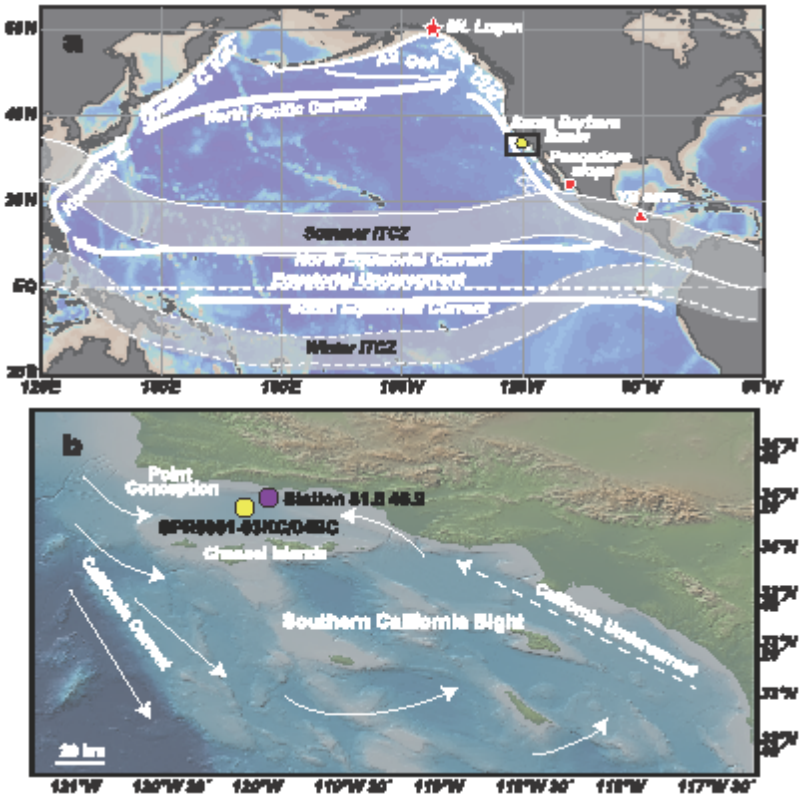

Figure 1. Core locations. a. Yellow circle: Core SPR0901-03KC (34° 16.99’ N, 120° 2.408’ W; 586 m depth) from the Santa Barbara Basin (SBB); red circle: Pescadero Slope core location from Tems et al. (2016). Red star: ice core location from Mt. Logan (Osterberg et al., 2014); red triangle: the YOK-I speleothem record from Belize (Kennett

et al., 2012). Summer and winter ITCZ positions are indicated in white belts bound by solid and dashed lines, respectively. Ocean currents are shown in white arrows. KaC: Kamchatka Current; Oyashio C: Oyashio Current; KuC: Kuroshio Current; CC: California Current; CUC: California Undercurrent; GoA: Gulf of Alaska; AC: Alaska Current; AS: Alaska Stream. b. Southern California Bight map corresponding to the black rectangle in a. The cores SPR0901-03KC and SPR0901-04BC (34°16.895' N, 120°2.489' W, 588 m water depth) are shown in the yellow circles. The CalCOFI Station 81.8 46.9 is represented by the purple circle, and the circulation pattern is modified from Hickey (1992). The base maps are generated from the Ocean data View in (a) and the GeoMapApp (http://www.geomapapp.org, Ryan et al. (2009)), respectively.

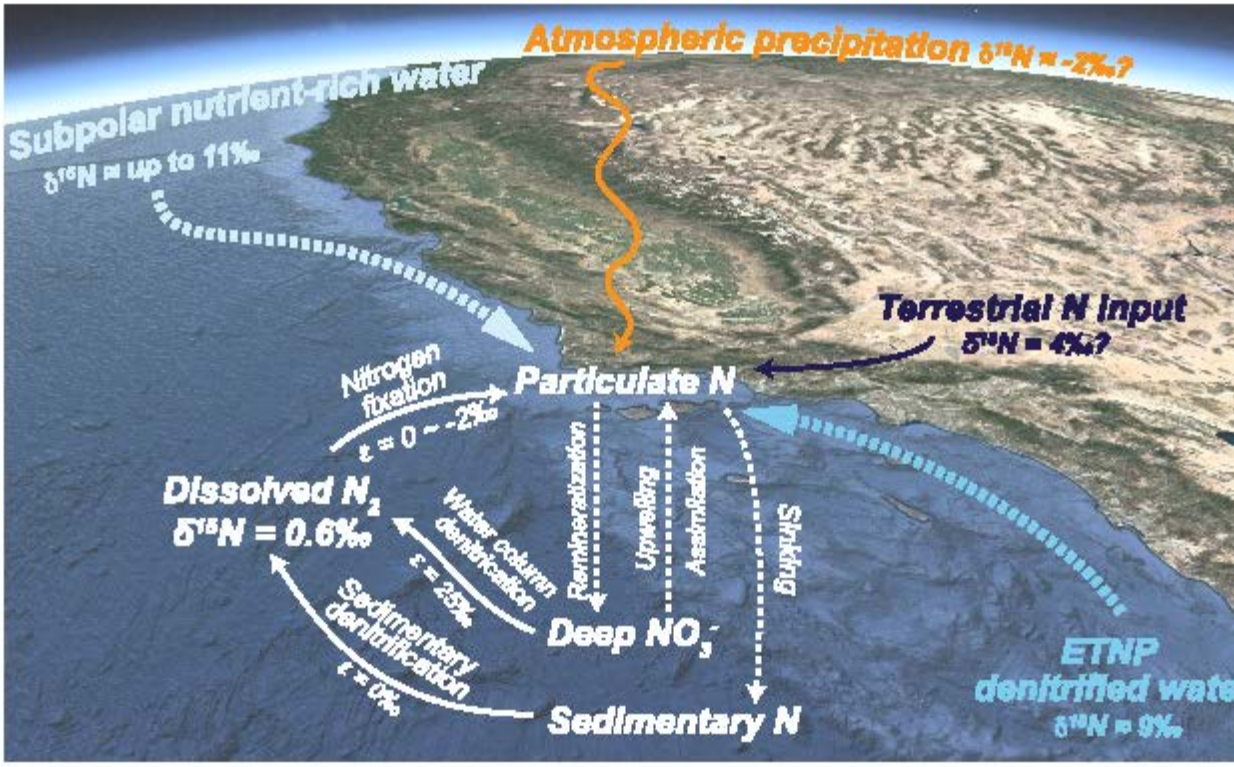

Figure 2. The nitrogen cycle in Southern California. Nitrogen inputs include dissolved N_2 via N fixation, atmospheric precipitation, terrestrial input, and remotely advected water masses (subpolar nutrient-rich waters and Eastern Tropical North Pacific [ETNP] dentrified waters shown in blue dashed arrows). Nitrogen outputs include water column

and sedimentary denitrification. Internal cycling (e.g., remineralization, assimilation) is denoted with white dashed arrows. Kinetic fractionation effects (ε) and isotopic values for major N sources and transformation pathways are labeled.

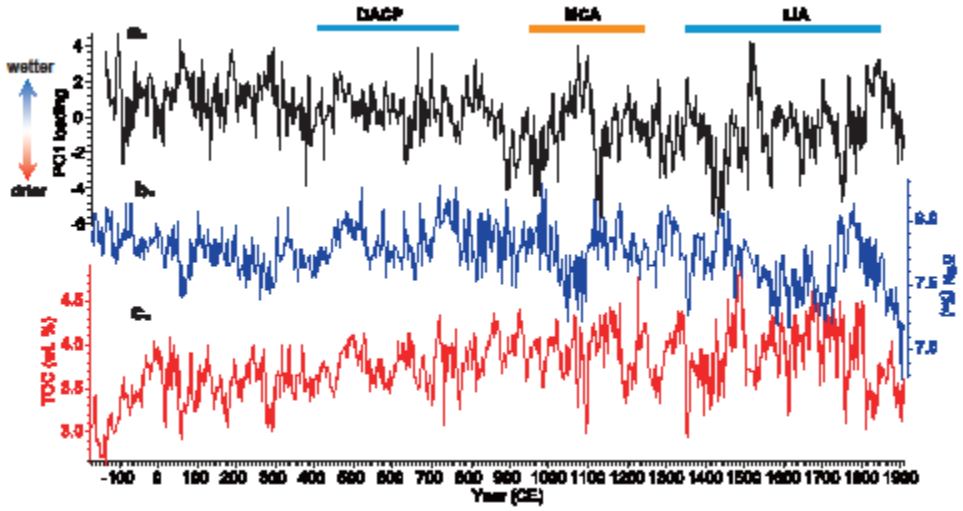

Figure 3. Local influences on $\delta^{15}N_{sed}$ in the Santa Barbara Basin. (a) The first principal component (PC1) of the scanning XRF elemental data for SPR0901-03KC (black line) used as a proxy for siliciclastic sediment derived from river runoff (Heusser et al., 2015). Higher PC1 indicates wetter conditions while low PC1 indicates drought; (b-c) $\delta^{15}N_{sed}$ (‰) (blue line) and TOC (wt. %) (red line) records from SPR0901-03KC, respectively. Blue bars indicate cool intervals: Dark Age Cold Period (DACP) and Little Ice Age (LIA). Red bars indicate warm intervals: Medieval Climate Anomaly (MCA). All instantaneous depositional events (flood and turbidite layers) have been removed.

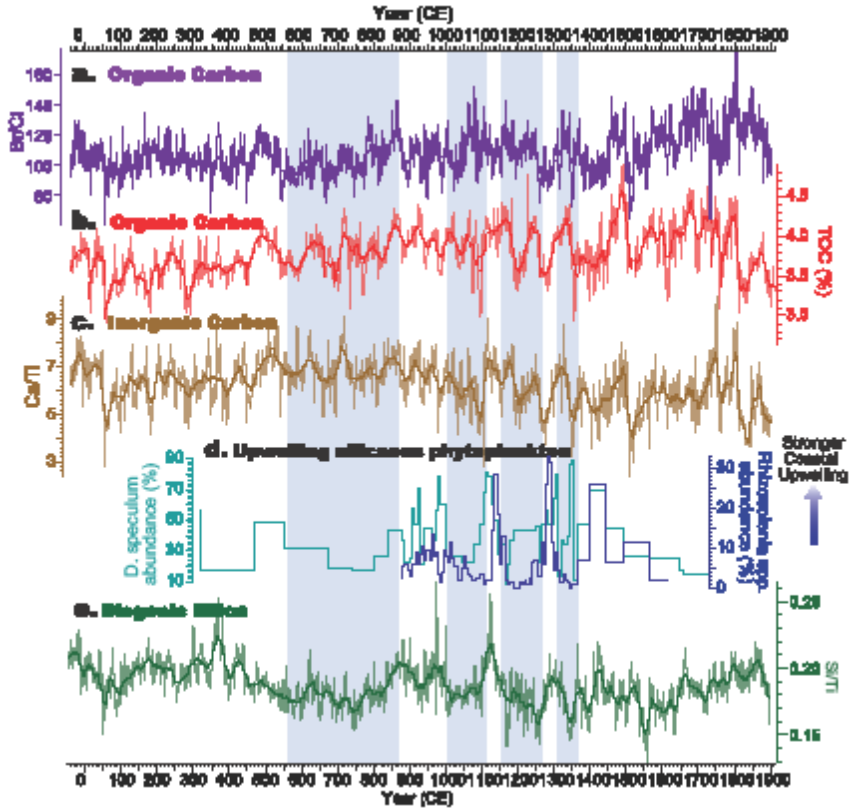

Figure 4. Productivity proxies. (a) Scanning XRF Br/Cl (proxy for organic carbon, thin purple line). Thick purple line represents the 101-point running mean; (b) TOC (wt. %) (thin red line) with 11-point running mean (thick red line); (c) scanning XRF of Ca/Ti (thin brown line) with the 101-point running mean (thick brown line); (d) upwelling diatoms and silicoflagellates from Barron et al. (2015); The teal and blue line represent the relative abundance of *Distephanus speculum* and *Rhizosolenia* spp., respectively; (e) proxy for biogenic silica, Si/Ti, from scanning XRF (thin green line) with the 101-point running mean (thick green line). Blue shaded rectangles indicate intervals of low coastal upwelling indicated from upwelling diatom and silicoflagellate abundance in (d).

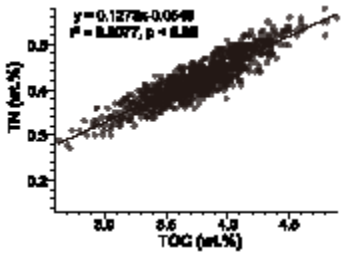

Figure 5. Cross plot of TOC (wt. %) and TN (wt. %) from SPR0901-03KC. Black line represents linear relationship from the least-square regression.

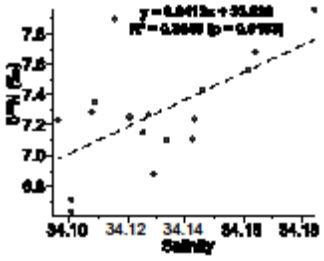

Figure 6. Cross plot of $\delta^{15}N_{sed}$ of the SBB core SPR0901-04BC (34° 16.895' N, 120° 02.489’ W, 588 m water depth) and mean annual salinity of σ_θ = 26.4-26.5 from the CalCOFI Station 81.8 46.9 (34° 16’29.64" N, 120° 1’30" W). The black dashed line shows the least-square regression.

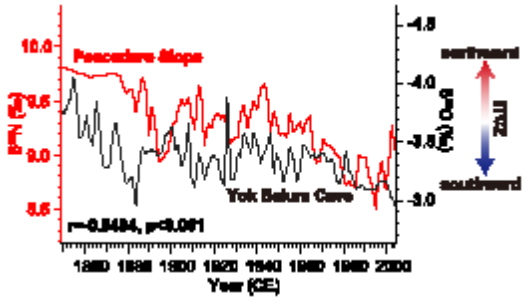

Figure 7. Comparison of $\delta^{15}N_{sed}$ of the Pescadero Basin (red line) with $\delta^{18}O$ of the Yok Balum Cave (YOK-I, black line, Kennett et al. (2012)) showing a statistically negative correlation (r=-0.5494, p<0.001).

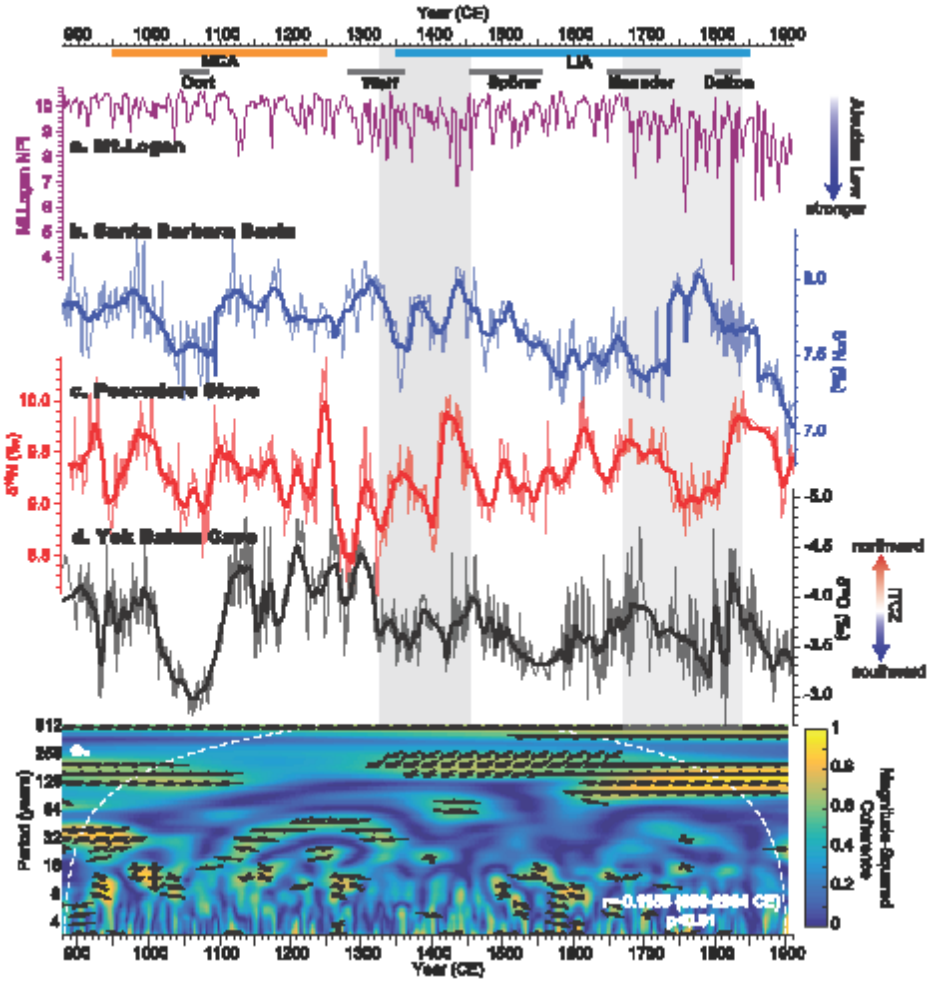

Figure 8. $\delta^{15}N$ regional comparison with North Pacific teleconnections. (a) Mt. Logan North Pacific Index proxy record (purple line, Osterberg et al. (2014)). Lower values indicate stronger winter Aleutian Low; (b) $\delta^{15}N_{sed}$ from SBB core SPR0901-03KC with the thick purple line showing the 11-point running mean to highlight multidecadal variability; (c) $\delta^{15}N_{sed}$ of the Pescadero Basin (Tems et al., 2016) with the thick red line denoting 11-point running mean; (d) YOK-I speleothem $\delta^{18}O$ as a proxy for ITCZ migration (Kennett et al., 2012). The 41-point running mean is shown in the black solid line. (e) Cross-wavelet coherence between $\delta^{18}O$ in (d) and Pescadero $\delta^{15}N_{sed}$ in (c). Arrows show phase differences between the two records when the magnitude-squared

coherence is above 0.5 (>95% significance). Arrows pointing left indicate anti-phase correlations at that frequency. The Medieval Climate Anomaly (MCA) and the Little Ice Age (LIA) are shown in orange and blue shaded bars, respectively. Grand solar minima are indicated with gray bars. Rectangles shaded in gray show time intervals where SBB and Pescadero $\delta^{15}N_{sed}$ records are not correlated.

References

Agnihotri, R., Altabet, M.A., Herbert, T.D., Tierney, J.E., 2008. Subdecadally resolved paleoceanography of the Peru margin during the last two millennia. Geochemistry, Geophysics, Geosystems, 9(5): n/a-n/a.

Altabet, M., 2006a. Constraints on oceanic N balance/imbalance from sedimentary 15N records. Biogeosciences Discussions, 3(4): 1121-1155.

Altabet, M.A., 2006b. Isotopic Tracers of the Marine Nitrogen Cycle: Present and Past. The Handbook of Environmental Chemistry, 2N: 251-293.

Altabet, M.A., François, R., 1994. Sedimentary nitrogen isotopic ratio as a recorder for surface nitrate utilization. Global Biogeochemical Cycles, 8(1): 103-116.

Altabet, M.A., Francois, R., Murray, D.W., Prell, W.L., 1995. Climate-related variations in denitrification in the Arabian Sea from sediment 15N/14N ratios. Nature, 373: 506-509.

Altabet, M.A., Murray, D.W., Prell, W.L., 1999a. Climatically linked oscillations in Arabian Sea denitrification over the past 1 m.y.: Implications for the marine N cycle. Paleoceanography, 14(6): 732-743.

Altabet, M.A. et al., 1999b. The nitrogen isotope biogeochemistry of sinking particles from the margin of the Eastern North Pacific. Deep Sea Research I, 46(1999): 655-679.

Bakun, A., 1973. Coastal upwelling indices, west coast of North America, 1946-71, NOAA, Seattle.

Barron, J.A., Bukry, D., 2007. Development of the California Current during the past 12,000 yr based on diatoms and silicoflagellates. Palaeogeography, Palaeoclimatology, Palaeoecology, 248(3-4): 313-338.

Barron, J.A., Bukry, D., Hendy, I.L., 2015. High-resolution paleoclimatology of the Santa Barbara Basin during the Medieval Climate Anomaly and early Little Ice Age based on diatom and silicoflagellate assemblages in Kasten core SPR0901-02KC. Quaternary International, 387: 13-22.

Blaauw, M., Christen, J.A., 2011. Flexible paleoclimate age-depth models using an autoregressive gamma process. Bayesian Analysis, 6(3): 457-474.

Bograd, S.J., Lynn, R.J., 2003. Anomalous subarctic influence in the southern California Current during 2002. Geophysical Research Letters, 30(15).
Brandes, J.A., Devol, A.H., Yoshinari, T., Jayakumar, D.A., Naqvi, S.W.A., 1998. Isotopic composition of nitrate in the central Arabian Sea and eastern tropical North Pacific: a tracer for mixing and nitrogen cycles. Limnology and Oceanography, 43(7): 1680-1689.
Broccoli, A.J., Dahl, K.A., Stouffer, R.J., 2006. Response of the ITCZ to Northern Hemisphere cooling. Geophysical Research Letters, 33(1): n/a-n/a.
Brown, E.T., Johnson, T.C., Scholz, C.A., Cohen, A.S., King, J.W., 2007. Abrupt change in tropical African climate linked to the bipolar seesaw over the past 55,000 years. Geophysical Research Letters, 34(20).
Bruland, K.W., Rue, E.L., Smith, G.J., 2001. Iron and macronutrients in California coastal upwelling regimes: Implications for diatom blooms. Limnology and Oceanography, 46(7): 1661-1674.
Canfield, D.E., 1994. Factors influencing organic carbon preservation in marine sediments. Chemical Geology, 114(3-4): 315-329.
Canfield, D.E., Thamdrup, B., Hansen, J.W., 1993. The anaerobic degradation of organic matter in Danish coastal sediments: iron reduction, manganese reduction, and sulfate reduction. Geochimica et Cosmochimica Acta, 57(16): 3867-3883.
Casciotti, K.L., Sigman, D.M., Hastings, M.G., Böhlke, J.K., Hilkert, A., 2002. Measurement of the oxygen isotopic composition of nitrate in seawater and freshwater using the denitrifier method. Analytical Chemistry, 74(19): 4905-4912.
Checkley, D.M., Barth, J.A., 2009. Patterns and processes in the California Current System. Progress in Oceanography, 83(1-4): 49-64.
Chelton, D.B., 1981. Interannual variability of the California Current - physical factors.
Chelton, D.B., 1984. Seasonal variability of alongshore geostrophic velocity off central California. Journal of Geophysical Research, 89(C3): 3473.
Chelton, D.B., Bernal, P.A., McGowan, J.A., 1982. Large-scale interannual physical and biological interaction in the California Current. Journal of Marine Research, 40: 1095-1125.
Chelton, D.B., Schlax, M.G., Samelson, R.M., 2007. Summertime Coupling between Sea Surface Temperature and Wind Stress in the California Current System. Journal of Physical Oceanography, 37(3): 495-517.
Chiang, J.C.H., Bitz, C.M., 2005. Influence of high latitude ice cover on the marine Intertropical Convergence Zone. Climate Dynamics, 25(5): 477-496.
Christoforou, P., Hameed, S., 1997. Solar cycle and the Pacific ‘centers of action'. Geophysical Research Letters, 24(3): 293-296.
Connolly, T.P., Hickey, B.M., Shulman, I., Thomson, R.E., 2014. Coastal Trapped Waves, Alongshore Pressure Gradients, and the California Undercurrent*. Journal of Physical Oceanography, 44(1): 319-342.

Consortium, P.k., 2013. Continental-scale temperature variability during the past two millennia. Nature Geoscience, 6(5): 339-346.
Costa, K.M. et al., 2017. Productivity patterns in the equatorial Pacific over the last 30,000 years. Global Biogeochemical Cycles, 31(5): 850-865.
Croudace, I.W., Rindby, A., Rothwell, R.G., 2006. ITRAX: description and evaluation of a new multi-function X-ray core scanner. Geological Society, London, Special Publications, 267(1): 51-63.
Cummins, P.F., Freeland, H.J., 2007. Variability of the North Pacific Current and its bifurcation. Progress in Oceanography, 75(2): 253-265.
Davis, C.V. et al., 2019. Ongoing increase in Eastern Tropical North Pacific denitrification as interpreted through Santa Barbara Basin sedimentary δ15N record. Paleoceanography and Paleoclimatology(Same issue).
Deutsch, C. et al., 2014. Centennial changes in North Pacific anoxia linked to tropical trade winds. Science, 345(6197): 665-668.
Deutsch, C., Sigman, D.M., Thunell, R.C., Meckler, A.N., Haug, G.H., 2004. Isotopic constraints on glacial/interglacial changes in the oceanic nitrogen budget. Global Biogeochemical Cycles, 18(4): n/a-n/a.
Di Lorenzo, E. et al., 2008. North Pacific Gyre Oscillation links ocean climate and ecosystem change. Geophysical Research Letters, 35(8).
Douglass, E., Roemmich, D., Stammer, D., 2006. Interannual variability in northeast Pacific circulation. Journal of Geophysical Research, 111(C4).
Du, X., Hendy, I., Schimmelmann, A., 2018. A 9000-year flood history for Southern California: A revised stratigraphy of varved sediments in Santa Barbara Basin. Marine Geology, 397: 29-42.
Enriquez, A.G., Friehe, C.A., 1995. Effects of wind stress and wind stress curl variability on coastal upwelling. Journal of Physical Oceanography, 25: 1651-1671.
Firme, G.F., Rue, E.L., Weeks, D.A., Bruland, K.W., Hutchins, D.A., 2003. Spatial and temporal variability in phytoplankton iron limitation along the California coast and consequences for Si, N, and C biogeochemistry. Global Biogeochemical Cycles, 17(1).
Freeland, H.J., 2003. Cold halocline in the northern California Current: An invasion of subarctic water. Geophysical Research Letters, 30(3).
Freeland, H.J., Cummins, P.F., 2005. Argo: A new tool for environmental monitoring and assessment of the world's oceans, an example from the N.E. Pacific. Progress in Oceanography, 64(1): 31-44.
Ganeshram, R.S., Pedersen, T.F., Calvert, S.E., François, R., 2002. Reduced nitrogen fixation in the glacial ocean inferred from changes in marine nitrogen and phosphorus inventories. Nature, 415: 156-159.

Ganeshram, R.S., Pedersen, T.F., Calvert, S.E., Murra, J.W., 1995. Large changes in oceanic nutrient inventories from glacial to interglacial periods. Nature, 376: 755-758.

Gay, P.S., Chereskin, T.K., 2009. Mean structure and seasonal variability of the poleward undercurrent off southern California. Journal of Geophysical Research, 114(C2).

Gómez-Valdivia, F., Parés-Sierra, A., Flores-Morales, A.L., 2015. The Mexican Coastal Current: A subsurface seasonal bridge that connects the tropical and subtropical Northeastern Pacific. Continental Shelf Research, 110: 100-107.

Gómez-Valdivia, F., Parés-Sierra, A., Laura Flores-Morales, A., 2017. Semiannual variability of the California Undercurrent along the Southern California Current System: A tropical generated phenomenon. Journal of Geophysical Research: Oceans, 122(2): 1574-1589.

Grinsted, A., Moore, J.C., Jevrejeva, S., 2004. Application of the cross wavelet transform and wavelet coherence to geophysical time series. Nonlinear Processes in Geophysics(11): 561-566.

Haug, G.H., Hughen, K.A., Sigman, D.M., Peterson, L.C., Röhl, U., 2001. Southward migration of the intertropical convergence zone through the Holocene. Science, 293(5533): 1304-1308.

Helama, S., Jones, P.D., Briffa, K.R., 2017. Dark Ages Cold Period: A literature review and directions for future research. The Holocene, 27(10): 1600-1606.

Hendy, I.L., Dunn, L., Schimmelmann, A., Pak, D.K., 2013. Resolving varve and radiocarbon chronology differences during the last 2000 years in the Santa Barbara Basin sedimentary record, California. Quaternary International, 310: 155-168.

Hendy, I.L., Napier, T.J., Schimmelmann, A., 2015. From extreme rainfall to drought: 250 years of annually resolved sediment deposition in Santa Barbara Basin, California. Quaternary International, 387: 3-12.

Heusser, L.E., Hendy, I.L., Barron, J.A., 2015. Vegetation response to southern California drought during the Medieval Climate Anomaly and early Little Ice Age (AD 800–1600). Quaternary International, 387: 23-35.

Hickey, B.M., 1978. The California current system—hypotheses and facts. Progress in Oceanography, 8(4): 191-279.

Hickey, B.M., 1992. Circulation over the Santa Monica-San Pedro Basin and Shelf. Progress in Oceanography, 30: 37-115.

Huyer, A., 2003. Preface to special section on enhanced Subarctic influence in the California Current, 2002. Geophysical Research Letters, 30(15).

Hwang, Y.-T., Frierson, D.M.W., Kang, S.M., 2013. Anthropogenic sulfate aerosol and the southward shift of tropical precipitation in the late 20th century. Geophysical Research Letters, 40(11): 2845-2850.

Ishi, Y., Hanawa, K., 2005. Large-scale variabilities of wintertime wind stress curl field in the North Pacific and their relation to atmospheric teleconnection patterns. Geophysical Research Letters, 32(10).

Jacobel, A.W., McManus, J.F., Anderson, R.F., Winckler, G., 2016. Large deglacial shifts of the Pacific Intertropical Convergence Zone. Nat Commun, 7: 10449.

Jacox, M.G., Moore, A.M., Edwards, C.A., Fiechter, J., 2014. Spatially resolved upwelling in the California Current System and its connections to climate variability. Geophysical Research Letters, 41(9): 3189-3196.

John, S.G., Mendez, J., Moffett, J., Adkins, J., 2012. The flux of iron and iron isotopes from San Pedro Basin sediments. Geochimica et Cosmochimica Acta, 93: 14-29.

Kennett, D.J. et al., 2012. Development and disintegration of Maya political systems in response to climate change. Science, 338(6108): 788-91.

Kienast, M. et al., 2005. On the sedimentological origin of down-core variations of bulk sedimentary nitrogen isotope ratios. Paleoceanography, 20(2): 1-13.

Kienast, S.S., Calvert, S.E., Pedersen, T.F., 2002. Nitrogen isotope and productivity variations along the northeast Pacific margin over the last 120 kyr: Surface and subsurface paleoceanography. Paleoceanography, 17(4): 7-1-7-17.

King, A.L., Barbeau, K.A., 2011. Dissolved iron and macronutrient distributions in the southern California Current System. Journal of Geophysical Research, 116(C3).

Koutavas, A., Lynch-Stieglitz, J., 2004. Variability of the Marine ITCZ over the Eastern Pacific during the Past 30,000 Years. In: Diaz, H.F., Bradley, R.S. (Eds.), The Hadley Circulation: Present, Past and Future. Advances in Global Change Research. Springer, Dordrecht, pp. 347-369.

Lechleitner, F.A. et al., 2017. Tropical rainfall over the last two millennia: evidence for a low-latitude hydrologic seesaw. Sci Rep, 7: 45809.

Liu, K.-K., Kaplan, I.R., 1989. The eastern tropical Pacific as a source of 15N ‐ enriched nitrate in seawater off southern California. Limnology and Oceanography, 34(5): 820-830.

Lynn, R.J., Simpson, J.J., 1987. The California Current System: The Seasonal Variability of its Physical Characteristics. Journal of Geophysical Research, 92(12): 12947-19966.

McClatchie, S. et al., 2016. The influence of Pacific Equatorial Water on fish diversity in the southern California Current System. Journal of Geophysical Research: Oceans, 121(8): 6121-6136.

McGee, D. et al., 2018. Hemispherically asymmetric trade wind changes as signatures of past ITCZ shifts. Quaternary Science Reviews, 180: 214-228.

Meehl, G.A., Arblaster, J.M., Branstator, G., van Loon, H., 2008. A Coupled Air–Sea Response Mechanism to Solar Forcing in the Pacific Region. Journal of Climate, 21(12): 2883-2897.

Meyers, P.A., 1997. Organic geochemical proxies of paleoceanographic, paleolimnologic, and paleoclimatic processes. Organic Geochemistry, 27(5/6): 213-250.

Moberg, A., Sonechkin, D.M., Holmgren, K., M., D.N., Karlén, W., 2005. Highly variable Northern Hemisphere temperatures reconstructed from low- and high-resolution proxy data. Nature, 433(7026): 613-617.

Müller, P.J., 1977. C/N ratios in Pacific deep-sea sediments: effect of inorganic ammonium and organic nitrogen compounds sorbed by clays. Geochimica et Cosmochimica Acta, 41(6): 765-776.

Münchow, A., 2000. Wind stress curl forcing of the coastal ocean near Point Conception, California. Journal of Physical Oceanography, 30: 1265-1280.

Murphree, T., Bograd, S.J., Schwing, F.B., Ford, B., 2003. Large scale atmosphere-ocean anomalies in the northeast Pacific during 2002. Geophysical Research Letters, 30(15).

Ortiz, J., Mix, A., Hostetler, S., Kashgarian, M., 1997. The California Current of the Last Glacial Maximum: Reconstruction at 42°N based on multiple proxies. Paleoceanography, 12(2): 191-205.

Ortiz, J.D., Mix, A.C., Collier, R.W., 1995. Environmental control of living symbiotic and asymbiotic foraminifera of the California Current. Paleoceanography, 10(6): 987-1009.

Osterberg, E.C. et al., 2014. Mount Logan ice core record of tropical and solar influences on Aleutian Low variability: 500–1998 A.D. Journal of Geophysical Research: Atmospheres, 119(19): 11189-11204.

Pérez-Cruz, L., 2017. Hydrological changes and paleoproductivity in the Gulf of California during middle and late Holocene and their relationship with ITCZ and North American Monsoon variability. Quaternary Research, 79(02): 138-151.

Philander, S.G.H., Gu, D., Lambert, G., Li, T., 1996. Why the ITCZ is mostly north of the equator. Journal of Climate, 9: 2958-2972.

Pichevin, L. et al., 2012. Silicic acid biogeochemistry in the Gulf of California: Insights from sedimentary Si isotopes. Paleoceanography, 27(2): n/a-n/a.

Pickett, M.H., 2003. Ekman transport and pumping in the California Current based on the U.S. Navy's high-resolution atmospheric model (COAMPS). Journal of Geophysical Research, 108(C10).

Pride, C. et al., 1999. Nitrogen isotopic variations in the Gulf of California since the Last Deglaciation: Response to global climate change. Paleoceanography, 14(3): 397-409.

Prokopenko, M. et al., 2006. Nitrogen cycling in the sediments of Santa Barbara basin and Eastern Subtropical North Pacific: Nitrogen isotopes, diagenesis and possible chemosymbiosis between two lithotrophs (Thioploca and Anammox)—"riding on a glider". Earth and Planetary Science Letters, 242(1-2): 186-204.

Reimer, P.J. et al., 2013. IntCal13 and Marine13 radiocarbon age calibration curves 0–50,000 years cal BP. Radiocarbon, 55(4): 1869-1887.

Reimers, C.E., Lange, C., Tabak, M., Bernhard, J., 1990. Seasonal spillover and varve formation in the Santa Barbara Basin, California. Limnology and Oceanography, 35(7): 1577-1585.

Ren, H. et al., 2017. 21st-century rise in anthropogenic nitrogen deposition on a remote coral reef. Science, 356(6339): 749-752.

Ridley, H.E. et al., 2015. Aerosol forcing of the position of the intertropical convergence zone since ad 1550. Nature Geoscience, 8(3): 195-200.

Rotstayn, L.D., Lohmann, U., 2002. Tropical Rainfall Trends and the indirect aerosol effect. Journal of Climate, 15: 2103-2116.

Ryan, W.B.F. et al., 2009. Global Multi-Resolution Topography synthesis. Geochemistry, Geophysics, Geosystems, 10(3): 1-9.

Rykaczewski, R.R., Checkley, D.M., Jr., 2008. Influence of ocean winds on the pelagic ecosystem in upwelling regions. Proc Natl Acad Sci U S A, 105(6): 1965-70.

Salvatteci, R. et al., 2014. The response of the Peruvian Upwelling Ecosystem to centennial-scale global change during the last two millennia. Climate of the Past, 10(2): 715-731.

Sarno, C.T. et al., 2019. The impacts of flood, drought, and turbidites on organic carbon burial over the past 2000 years in the Santa Barbara Basin, California. Paleoceanography and Paleoclimatology(same issue).

Schimmelmann, A., 2011. The “coffin lid” effect: flood layers and turbidites in Santa Barbara Basin affect diagenesis of organic matter in underlying varved sediment. In: Besonen, M.R. (Editor), Second Workshop of the PAGES Varves Working Group, Corpus Christi, Texas, USA, pp. 83-86.

Schimmelmann, A. et al., 1992. Extreme climatic conditions recorded in Santa Barbara Basin laminated sediments: the 1835–1840 Macoma event. Marine Geology, 106(1992): 279-299.

Schimmelmann, A., Lange, C.B., Berger, W.H., 1990. Climatically controlled marker layers in Santa Barbara Basin sediments and fine-scale core-to-core correlation. Limnology and Oceanography, 35(1): 165-173.

Schneider, T., Bischoff, T., Haug, G.H., 2014. Migrations and dynamics of the intertropical convergence zone. Nature, 513(7516): 45-53.

Schubert, C.J., Calvert, S.E., 2001. Nitrogen and carbon isotopic composition of marine and terrestrial organic matter in Arctic Ocean sediments: implications for nutrient utilization and organic matter composition. Deep Sea Research I, 48(3): 789-810.

Sigman, D.M., Karsh, K.L., Casciotti, K.L., 2009a. Nitrogen Isotopes in the Ocean, Encyclopedia of Ocean Sciences (Second Edition). Academic Press, Oxford, pp. 40-54.

Sigman, D.M., Karsh, K.L., Casciotti, K.L., 2009b. Ocean process tracers: nitrogen isotopes in the ocean.

Strub, P.T., James, C., 2003. Altimeter estimates of anomalous transports into the northern California Current during 2000-2002. Geophysical Research Letters, 30(15).

Sydeman, W.J. et al., 2011. Does positioning of the North Pacific Current affect downstream ecosystem productivity? Geophysical Research Letters, 38(12): 1-6.

Taylor, A.G., Landry, M.R., Selph, K.E., Wokuluk, J.J., 2015a. Temporal and spatial patterns of microbial community biomass and composition in the Southern California Current Ecosystem. Deep Sea Research Part II: Topical Studies in Oceanography, 112: 117-128.

Taylor, M.A., Hendy, I.L., Pak, D.K., 2015b. The California Current System as a transmitter of millennial scale climate change on the northeastern Pacific margin from 10 to 50 ka. Paleoceanography, 30(9): 1168-1182.

Tems, C.E. et al., 2016. Decadal to centennial fluctuations in the intensity of the eastern tropical North Pacific oxygen minimum zone during the last 1200 years. Paleoceanography, 31(8): 1138-1151.

Thunell, R., Benitez-Nelson, C., Varela, R., Astor, Y., Muller-Karger, F., 2007. Particulate organic carbon fluxes along upwelling-dominated continental margins: Rates and mechanisms. Global Biogeochemical Cycles, 21(1).

Thunell, R.C., 1998a. Particle fluxes in a coastal upwelling zone: sediment trap results from Santa Barbara Basin, California. Deep Sea Research Part II: Topical Studies in Oceanography, 45(8): 1863-1884.

Thunell, R.C., 1998b. Seasonal and annual variability in particle fluxes in the Gulf of California: A response to climate forcing. Deep Sea Research Part I: Oceanographic Research Papers, 45(12): 2059-2083.

Thunell, R.C., Sigman, D.M., Muller-Karger, F., Astor, Y., Varela, R., 2004. Nitrogen isotope dynamics of the Cariaco Basin, Venezuela. Global Biogeochemical Cycles, 18(3): 1-13.

Thunell, R.C., Tappa, E.J., Andersen, D.M., 1995. Sediment fluxes and varve formation in Santa Barbara Basin, offshore California. Geology, 23(12): 1083-1086.

Torrence, C., Compo, G.P., 1997. A practical guide to wavelet analysis. Bulletin of the American Meteorological Society, 79(1): 61-78.

Warrick, J.A., Farnsworth, K.L., 2009a. Dispersal of river sediment in the Southern California Bight. 454: 53-67.

Warrick, J.A., Farnsworth, K.L., 2009b. Sources of sediment to the coastal waters of the Southern California Bight. The Geological Society of America Special Paper, 454: 39-52.

Xie, S.-P., 1994. Oceanic response to the wind forcing associated with the Intertropical Convergence Zone in the northern hemisphere. Journal of Geophysical Research, 99(C10): 20393.